

Selected Papers

Electron Conductivity in Modified Models of Artificial Metal–DNA Using Green's Function-Based Elastic Scattering Theory

Yasuyuki Nakanishi,*[1] Toru Matsui,[2] Yasutaka Kitagawa,[1] Yasuteru Shigeta,[2] Toru Saito,[1] Yusuke Kataoka,[1] Takashi Kawakami,[1] Mitsutaka Okumura,[1] and Kizashi Yamaguchi[1]

[1]Department of Chemistry, Graduate School of Science, Osaka University, 1-1 Machikaneyama, Toyonaka, Osaka 560-0043

[2]Division of Chemical Engineering, Department of Materials Engineering Science, Graduate School of Engineering Science, Osaka University, 1-1 Machikaneyama, Toyonaka, Osaka 560-0043

Received July 22, 2010; E-mail: y-naka@chem.sci.osaka-u.ac.jp

In this paper, we investigate the current–voltage (*I–V*) characteristics between adjacent bases in two types of artificial metal–DNA (M–DNA) models, i.e., hydroxypyridone (=2-methyl-3-hydroxy-4-pyridone, **H**) and salen (=*N*,*N*′-bis(salicylidene)ethylenediamine, **S**) complexes, using an elastic scattering Green's function method together with a density functional theory. In order to estimate quantitative behaviors of the *I–V* characteristics of the artificial M–DNAs, we considered *I–V* characteristics from the following viewpoints: the effect of spin states, the effect of backbone, and the effect of metal ions. We have found that the magnitude of the current of the **H** complex tends to become larger than that of the **S** complex. We also found that a difference in the spin states drastically changes the *I–V* characteristics. These behaviors suggest the possibility of the control of the *I–V* characteristics in the artificial M–DNA by an external magnetic field.

Molecular devices have attracted much attention in nanoelectronics because of a limitation on a miniaturization of conventional silicon-based devices. For example, it is expected that a top down approach reaches a drastic limit at 100 nm.[1] In molecular devices, especially in a molecular wire, a delocalization of a π-electron cloud is useful for electron conductivity. On the other hand, DNA is well known not only as the molecule containing all genetic information, but also as a possible candidate for molecular wire along the π-stacking axis. In order to utilize DNA for molecular wire, a large number of studies on the mechanism of electron transfer in DNA have been reported.[2–12] However, little is known about whether DNA is a conductor or not. Zhang et al. observed low electron conductivity of DNA wire, and concluded that it was a typical insulator.[6] On the other hand, Kasumov et al. reported that DNA molecules could be a good conductor.[10] From theoretical studies, Tada et al. reported that DNA molecules were semiconductors if the base was directly connected with gold leads, but were insulators if the sugar–phosphates were connected with gold leads.[11] In this way, there are contrary observations of the DNA conductors.

On the other hand, there have been several attempts to synthesize novel DNA-based compounds to achieve DNA conductors. One promising candidate is a metal-complexed DNA (M–DNA). This system is expected to conduct an electric current through redox of the metal atom. Coordination of DNA to metal ions causes a change in the structure and physical properties. Particularly, the complex formation sometimes leads to the double-helical structure of DNA becoming loose, and that the linear one-dimensional chain of the DNA duplex is damaged by the large transformation. For example, cisplatin, which is known as an anticancer drug, attaches to the outer region of the DNA duplex and distorts the structure of the duplex.[13–16] Therefore it is thought to be a unproductive to arrange metal ions on the outside of DNA duplexes. Meanwhile, incorporation of metal ions into the inner region of DNA duplexes has been attempted in recent years. One of the examples is an artificial M–DNA.

As mentioned above, DNA has a double-helical structure made from a complementary hydrogen-bonding pair called the Watson–Crick base pair, and is stabilized by a π–π stacking interaction. Tanaka et al. succeeded in making complexes by putting Cu^{2+} ions into the DNA double helix using hydroxypyridone (=2-methyl-3-hydroxy-4-pyridone, **H**) ligand as an artificial nucleoside.[17] Here, it is transcribed as **H**–Cu^{2+}–**H**. The merit of the material is the replacement of the Watson–Crick base pair in the natural DNA by the coordinate bond of metal.[18] A ferromagnetic interaction between electron spins on adjacent Cu^{2+} ions has also been found by electron paramagnetic resonance (EPR) spectra,[17] suggesting that this has a possibility for spintoronics[19] of DNA wire. From these points of view, it is interesting to investigate magnetism and the electron transport in this system.

The first theoretical calculation of the magnetism of this system was reported by Zhang et al.[20] They showed that the ferromagnetic (F) and the antiferromagnetic (AF) phases were

Published on the web March 30, 2011; doi:10.1246/bcsj.20100207

energetically almost degenerate. Jishi et al. also calculated the total energy of [**H**–Cu^{2+}–**H**] with three different symmetries.[21] On the other hand, our group demonstrated that the thermal excitation from the antiferromagnetic (AF) state to the ferromagnetic (F) state would occur in the system by Boltzmann distribution simulation based on a simulation with calculated effective exchange integral (J_{ab}) values.[22] Mallajosyula and Pati also reported that optical conductivity showed a peak of a low frequency excitation at 0.8 eV.[23] In addition, according to our previous density functional theory (DFT) studies[24] with an Anderson–Langreth–Lindqvist van der Waals (vdW) functional,[25] the spin–spin interaction among Cu^{2+} ions was not important for the stacking stabilization of **H**–Cu^{2+}–**H**, and we could reproduce the experimental distance between Cu^{2+} ions.

Another development of an artificial M–DNA was carried out by Clever et al. using salen (=*N*,*N*′-bis(salicylidene)ethylenediamine, **S**) ligand in which a variety of metal ions could be introduced as coordination partners.[26,27] An advantage of the salen ligand is that the ethylenediamine, which is used to assemble the metal–salen complexes inside the DNA double strand, forms a covalent crosslink, and brings a high stability to the duplex. This system showed a weak antiferromagnetic interaction from theoretical studies.[28,29] Afterward, Clever et al. reported that this system experimentally showed antiferromagnetic interaction.[30,31]

Our other interest in the artificial M–DNAs is to calculate the *I–V* characteristics. Up to now, various artificial M–DNAs[32,33] and artificial nucleosides[34–38] have been reported. However, the electron conductivities of artificial M–DNA have not been reported yet in spite of the many reports of the electron conductivity of natural DNA. Therefore, it is necessary to examine the electron conductivity of artificial M–DNAs to understand the effect of metal ions and so on. Mallajosyula and Pati also have pointed out the importance from a theoretical perspective.[39]

The elastic scattering approach from the original work by Mujica et al. is often used to investigate the *I–V* characteristics between two reservoirs with each electronic state at the two terminals of the molecular wire.[40–42] However, it is difficult to calculate the *I–V* characteristics for large systems that consist of many atoms in their approach, because it needs quite high computational resources. For that reason, Luo et al. modified the approach with a simple model which uses (1) the overlap matrix elements, (2) the terminated atoms connected to the reservoirs, and (3) the probabilities that the electrons exist at the terminal atoms within LUMO.[43–45] In the paper, they demonstrated that the calculated results agreed with experimental results of the *I–V* characteristics for a benzenedithiol molecule. They also succeeded in the calculation of the molecular electron conductance of the vertical distance between two aromatic molecules. From both points of view, i.e., the computational costs and the quantitativeness, we decided to modify this method and to apply it to the investigation of artificial M–DNAs.

Because of the above reasons, this paper aims to investigate the *I–V* characteristics of the artificial M–DNAs, [**H**–Cu^{2+}–**H**] and [**S**–Cu^{2+}–**S**] systems. Effects of spin states, metal ions, and the backbone are examined by using the elastic scattering Green's function approach based on DFT.

We first extended Luo's elastic scattering Green's function theory to an open-shell system in order to compute the *I–V* characteristics of the artificial M–DNAs using the broken-symmetry (BS) DFT results. The difference in the *I–V* characteristics between high-spin (HS) and BS low-spin (LS) states was investigated because the existence of electron spins played a key role in these systems. The HS state means that the localized spins on two Cu^{2+} ions of adjacent molecules are in parallel state (ferromagnetic interaction), and the BS LS state means an untiparallel state (antiferromagnetic interaction). Hereafter, we use these definitions. To our knowledge, no one has ever reported the comparison of the HS with the BS LS results of the *I–V* characteristics. Finally, it should be noted that there are many calculated reports about electron structures of DNA using the DFT method, which does not involve π–π interaction well, but those results indicate that the density matrix of the DFT can be applicable to a qualitative discussions of the properties (for example, see Refs. 12 and 46). In addition, it is also important for the electron transport in DNA to consider the effect of water molecules and counter ions, although we carried out all calculations in the gas phase, as a first step for the elucidation of the electron conductivity of these systems.

Theoretical Background

The elastic scattering theory proposed by Luo et al.[43,44] was originally developed for closed-shell systems, so we extend the method to open-shell systems. The Hamiltonian of the system is written as

$$
\begin{aligned}
H &= H_{\mathrm{M}} + H_{\mathrm{L}} + H_{\mathrm{R}} + U,\\
H_{\mathrm{M}} &= \sum_{\sigma=\pm}\sum_{\alpha} E^0_{\alpha\sigma}|\alpha_\sigma\rangle\langle\alpha_\sigma| \equiv \sum_{\sigma=\pm}\sum_{\alpha} E^0_{\alpha\sigma} C^*_{\alpha\sigma I} C_{\alpha\sigma J}|I\rangle\langle J|,\\
H_{\mathrm{L}} &= \sum_{\sigma=\pm}\sum_{i} E^0_{i\sigma}|i_\sigma\rangle\langle i_\sigma|,\\
H_{\mathrm{R}} &= \sum_{\sigma=\pm}\sum_{j} E^0_{j\sigma}|j_\sigma\rangle\langle j_\sigma|,\\
U &= \sum_{\sigma=\pm}\sum_{I}\left(\sum_{i}\gamma_{iI,\sigma}|i_\sigma\rangle\langle I| + \sum_{j}\gamma_{jI,\sigma}|j_\sigma\rangle\langle I|\right) + c.c. \quad (1)
\end{aligned}
$$

where H_{M} and $H_{\mathrm{L(R)}}$ are the Hamiltonians of the molecule and the left (right) side reservoirs, respectively. U is the interaction potential between the molecule and the reservoirs and $\gamma_{il,\sigma}$ represents the interaction between the *I*-th site of molecule and the *i*-th orbital of the reservoirs with spin σ.

In the elastic scattering Green's function theory, the transition operator[47–49] ($\mathscr{T}$) is defined as

$$\mathscr{T} = U + UGU \quad (2)$$

Assuming that only the reservoirs directly interact with the end-sites (site 1 and N) of the molecule,[40,50] the transition matrix element ($\mathscr{T}_{ij,\sigma}$) can be rewritten as

$$
\begin{aligned}
\mathscr{T}_{ij,\sigma}(z) &= \gamma_{i1,\sigma} G_{1N,\sigma}(z) \gamma_{Nj,\sigma},\\
G_{1N,\sigma}(z) &= \sum_{p}\left\langle 1\left|\frac{1}{z-H}\right|\phi_{p,\sigma}\right\rangle\langle\phi_{p,\sigma}|N\Big\rangle\\
&= \sum_{p}\frac{\langle 1|\phi_{p,\sigma}\rangle\langle\phi_{p,\sigma}|N\rangle}{z-\varepsilon_{p,\sigma}}
\end{aligned}
$$

$$\approx \sum_{\eta}\sum_{p}\frac{\langle 1|\phi_{p,\sigma}\rangle\langle\phi_{p,\sigma}|N\rangle}{z-\varepsilon^{\eta}_{p,\sigma}} \quad (3)$$

where $\{|\phi_{p,\sigma}\rangle\}$ is the eigenstate of the total Hamiltonian H ($H|\phi_{p,\sigma}\rangle = \varepsilon_{p,\sigma}|\phi_{p,\sigma}\rangle$). Here, the end-site is defined as the terminal atom connected to the reservoir as explained above. The eigenstate p that overlaps with the molecular end-sites only contributes to the Green's function matrix element significantly. Therefore, $\{|\phi_{p,\sigma}\rangle\}$ can be approximated by orbitals obtained from the Kohn–Sham equation of a finite system consisting of the molecule sandwiched between reservoirs ($H|\phi_{p,\sigma}\rangle = \varepsilon^{\eta}_{p,\sigma}|\phi_{p,\sigma}\rangle$).[43]

In the linear response theory, the current density[51] (i^{LR}_{σ}) of the system that are applied the voltage (V_{D}) by right and left reservoirs is given as

$$i^{\mathrm{LR}}_{\sigma} = \frac{1}{2}\sum_{\eta}\frac{emk_{\mathrm{B}}T}{2\pi^2\hbar^3}\int_{eV_{\mathrm{D}}}^{\infty}\mathrm{d}E|\mathscr{T}_{\sigma}(E)|^2_{\eta}f_{\sigma}(E),$$

$$f_{\sigma}(E) = \left\{\ln\left[1+\exp\left(\frac{E_{\mathrm{F},\sigma}+eV_{\mathrm{D}}-E}{k_{\mathrm{B}}T}\right)\right] - \ln\left[1+\exp\left(\frac{E_{\mathrm{F},\sigma}-E}{k_{\mathrm{B}}T}\right)\right]\right\} \quad (4)$$

where E_{F} is the Fermi energy. Here, we define the intermediate value of HOMO and LUMO orbital energies of the extended molecular system as the Fermi energy. Since the spacing between molecular orbitals is large, we can assume that the interference between different scattering channels is negligible.[43] Then $|\mathscr{T}(E)|^2_{\sigma}$ represents the transition probability,

$$|\mathscr{T}_{\sigma}(E)|^2 = \gamma^2_{\mathrm{L1},\sigma}\gamma^2_{N\mathrm{R},\sigma}\sum_{\eta}\frac{|\langle 1|\phi_{p,\sigma}\rangle|^2|\langle\phi_{p,\sigma}|N\rangle|^2}{(\varepsilon^{\eta}_{p,\sigma}-E)^2+\Gamma^2_{p,\sigma}} \quad (5)$$

where $\Gamma_{p,\sigma}$ denotes the spin-dependent escape rate determined by the Fermi golden rule, i.e.,

$$\Gamma_{p,\sigma} = \frac{\gamma_{\mathrm{L1},\sigma}\langle 1|\phi_{p,\sigma}\rangle + \gamma_{N\mathrm{R},\sigma}\langle\phi_{p,\sigma}|N\rangle}{2} \quad (6)$$

$\langle 1|\phi_{p,\sigma}\rangle$ and $\langle\phi_{p,\sigma}|N\rangle$ represent the site-orbital overlap matrix elements between the end-sites and the extended molecule. The product of two site-orbital overlap matrixes represents the delocalization of the molecular orbital of the extended molecule. In this paper, we adopt the orbitals from HOMO−9 to LUMO+9 as the orbitals concerned with the conductivity.

γ is a parameter to determine the *I–V* characteristic and it is in proportion to a transition probability. To determine the γ parameter, on the assumption of the Dewar, Chatt, and Duncanson (DCD) model,[52,53] Luo et al. proposed a procedure that the occupied orbitals of the reservoirs interacted with LUMO of the molecule according to frontier orbital theory.[44] Therefore, γ can be written as

$$\gamma_{\mathrm{L1},\sigma}(\mathrm{LUMO}) = V_{\mathrm{L},\sigma}(\mathrm{LUMO})d^{*}_{1,\sigma}(\mathrm{LUMO}) \quad (7)$$

$$V^2_{\mathrm{L},\sigma}(\mathrm{LUMO}) = \frac{(\Delta E_{\sigma,\mathrm{HOMO\text{–}LUMO}} - \Delta E_{\sigma,\mathrm{LUMO}})\Delta E_{\sigma,\mathrm{LUMO}}}{2} \quad (8)$$

$$d^2_{1,\sigma}(\mathrm{LUMO}) = \frac{\sum_{i} c^2_{1,i,\sigma}}{\sum_{a,i} c^2_{a,j,\sigma}} \quad (9)$$

where $\Delta E_{\sigma,\mathrm{HOMO\text{–}LUMO}}$ is the HOMO–LUMO gap of the extended molecule and $\Delta E_{\sigma,\mathrm{LUMO}}$ is the energy difference between the HOMO of the $d^2_{1,\sigma}$(LUMO) reservoirs (gold clusters) and the LUMO of the isolated molecule which is not connected with the reservoirs. is the square of an expansion coefficient of the wave function of the isolated molecule at the end-site.

In the system where the LUMO of the molecule is not degenerate, we can use eqs 7–9. However, we cannot apply the equations to the degenerate LUMO. So in the system we extend the equations to the degenerate system using the Boltzmann distribution. Here, assuming that eq 7 can apply to the degenerate LUMO, eqs 7–9 becomes the following,

$$\gamma_{\mathrm{L1},\sigma} = V_{\mathrm{L},\sigma}d^{*}_{1,\sigma} \quad (10)$$

$$V_{\mathrm{L},\sigma} \approx V_{\mathrm{L},\sigma}(\mathrm{LUMO}) \quad (11)$$

$$d^{*}_{1,\sigma} = \frac{\sum_{k}\exp[-(E_{\mathrm{LUMO}+k}-E_{\mathrm{LUMO}})/RT]d_{\mathrm{LUMO}+k}}{\sum_{k}\exp[-(E_{\mathrm{LUMO}+k}-E_{\mathrm{LUMO}})/RT]} = \frac{\sum_{k}B_k d_{\mathrm{LUMO}+k}}{\sum_{k}B_k} \quad (12)$$

where k means the number of degenerate orbitals around LUMO and B_k is a parameter calculated by the Boltzmann distribution. In $k=0$, (that is, the nondegenerate LUMO), eqs 10–12 are equal to eqs 7–9. Here, this approach is based on the single reference method but not on the multireference method as shown in eq 3.

The total current is $I^{\mathrm{LR}}_{\sigma} = Ai^{\mathrm{LR}}_{\sigma}$, where A is the effective injection area, $A \approx \pi r^2_{\sigma}$.[43] Here, r_{σ} is defined by $r_{\sigma} = [3/(4\pi N_{\sigma})]^{1/3}$ and the density of electron is $N_{\sigma} = (2mE_{\sigma,\mathrm{F}})^{3/2}/(3\hbar^3\pi)$.

Computational Details

In this study, we examined the *I–V* characteristics of two types of artificial M–DNAs, hydroxypyridone (**H**)[17] and salen (**S**)[27] complexes. In order to calculate the *I–V* characteristics for both of the systems, we first optimized the geometry of monomer structures of [**H**–Cu^{2+}–**H**] and [**S**–Cu^{2+}–**S**], where [**X**–Cu^{2+}–**X**] (**X** = **H** and **S**) means one monomer. As model structures, the backbone was replaced by S atoms.

The dimer models for both of the systems were constructed by using those monomers. We assumed that the rotation angle was 36° clockwise. The distances of adjacent planes of [**H**–Cu^{2+}–**H**]$_2$ and [**S**–Cu^{2+}–**S**]$_2$ are 3.7 Å[17] and 3.375 Å,[27,54] respectively. The bond lengths of Au–Au and the distance between a S atom and the gold cluster surface is fixed to 2.88 and 2.3 Å, respectively.[44] Finally, the models of the artificial M–DNAs were connected to the hollow site of Au(111) surface as illustrated in Figure 1. As mentioned above, we used the results of DFT calculations for the *I–V* characteristics simulations. These calculations were performed by UB3LYP[55] on the Gaussian03 program package.[56] Basis sets used for the ligands were 6-31G* for the geometry optimization and 6-31+G* for the single point energy calculations. Huzinaga MIDI+pd basis set[57] and LANL2DZ were used for Cu and Au atoms, respectively. We set the temperature at 300 K to evaluate the *I–V* characteristics.

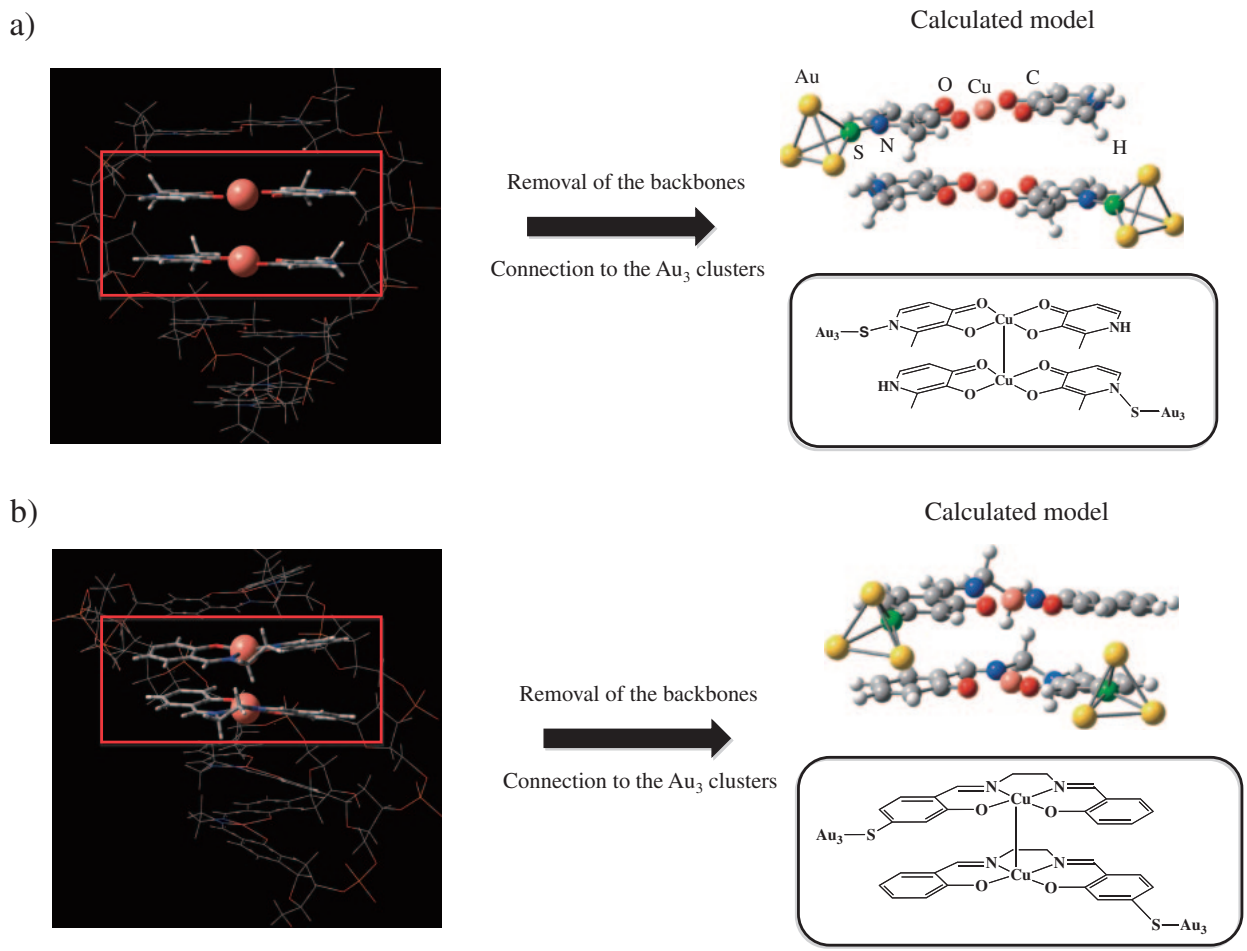

Figure 1. The calculated dimer models of Cu^{2+}-mediated base pairs of a) [**H**–Cu^{2+}–**H**]$_2$ and b) [**S**–Cu^{2+}–**S**]$_2$. The backbone is replaced by S atoms in the models and connected to the hollow site model structures on Au(111) surface.

Table 1. The Coupling Constants γ of Each Orbital for [**H**–Cu^{2+}–**H**]$_2$ and [**S**–Cu^{2+}–**S**]$_2$ in the HS and the BS LS States[a)]

HS				BS			
α orbital		β orbital		α orbital		β orbital	
[**H**–Cu^{2+}–**H**]$_2$							
$\gamma_{1R(\alpha)}$/eV	0.207	$\gamma_{1R(\beta)}$/eV	0.210	$\gamma_{1R(\alpha)}$/eV	0.097	$\gamma_{1R(\beta)}$/eV	0.274
$\gamma_{LN(\alpha)}$/eV	0.336	$\gamma_{LN(\beta)}$/eV	0.312	$\gamma_{LN(\alpha)}$/eV	0.197	$\gamma_{LN(\beta)}$/eV	0.258
γ_α/eV	0.070	γ_β/eV	0.066	γ_α/eV	0.019	γ_β/eV	0.071
[**S**–Cu^{2+}–**S**]$_2$							
$\gamma_{1R(\alpha)}$/eV	0.127	$\gamma_{1R(\beta)}$/eV	0.212	$\gamma_{1R(\alpha)}$/eV	0.068	$\gamma_{1R(\beta)}$/eV	0.199
$\gamma_{LN(\alpha)}$/eV	0.154	$\gamma_{LN(\beta)}$/eV	0.263	$\gamma_{LN(\alpha)}$/eV	0.081	$\gamma_{LN(\beta)}$/eV	0.256
γ_α/eV	0.020	γ_β/eV	0.056	γ_α/eV	0.006	γ_β/eV	0.051

a) $\gamma_\alpha = \gamma_{1R(\alpha)}\gamma_{LN(\alpha)}$, $\gamma_\beta = \gamma_{1R(\beta)}\gamma_{LN(\beta)}$.

Results and Discussion

Comparison of the High-Spin State with the Broken-Symmetry Low-Spin State. In this section, we explain the results of the *I–V* characteristics especially in terms of a comparison between the HS and the BS LS states.

We summarized the calculated coupling constant (γ) values in Table 1 and the current values at 1 V in Table 2 for the HS and the BS LS states. In the [**H**–Cu^{2+}–**H**]$_2$ model, LUMO and LUMO+1 are degenerate, so we adopted both LUMO and LUMO+1 for the calculation of the coupling constants. On the other hand, in the [**S**–Cu^{2+}–**S**]$_2$ model, we included from LUMO to LUMO+3. As mentioned above, the DFT results are utilized i.e., Kohn–Sham orbital energies and the site-orbital overlap matrix elements (simply transcribed as overlap element hereafter) for these calculations. These parameters are summa-

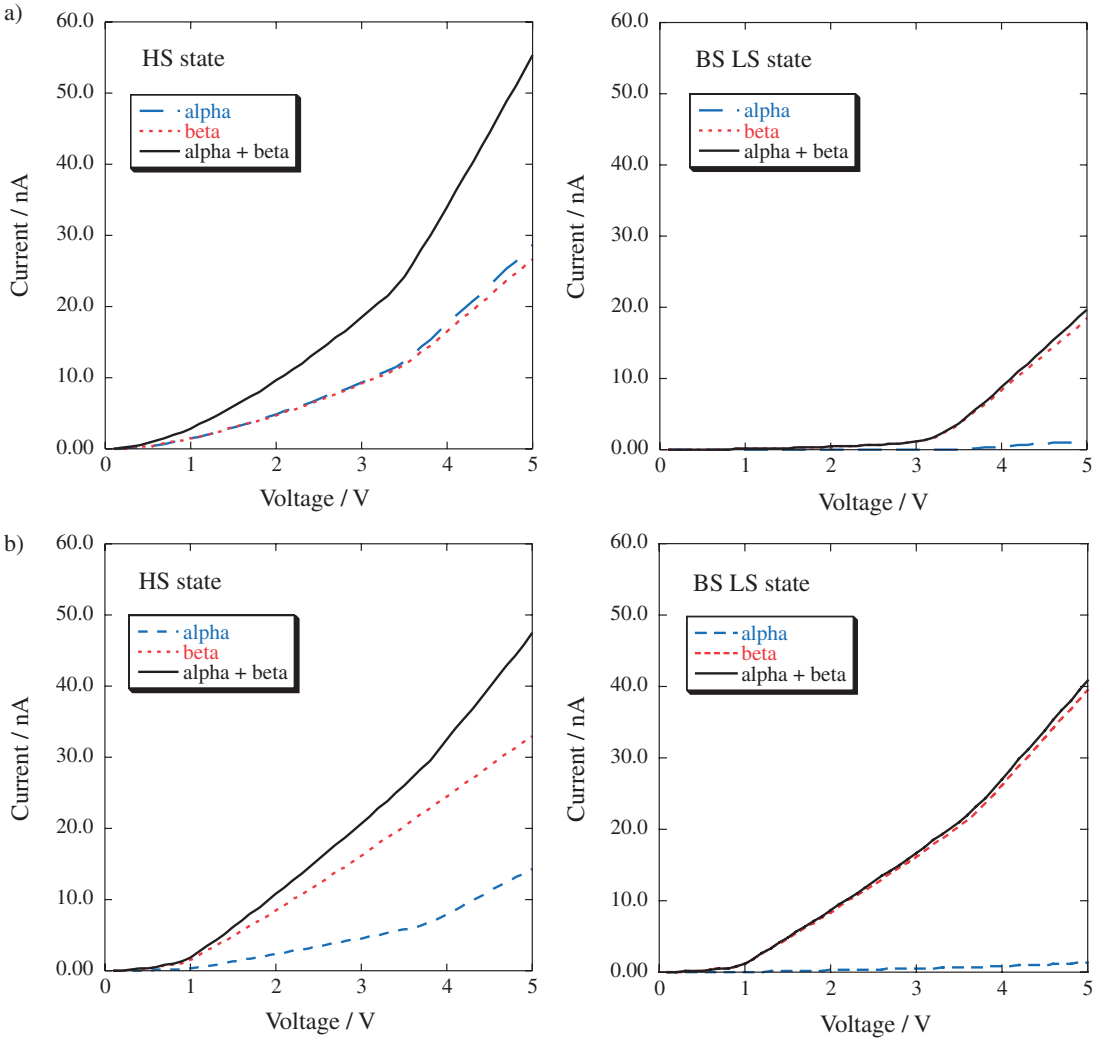

Figure 2. *I–V* curves of a) [**H**–Cu^{2+}–**H**]$_2$ and b) [**S**–Cu^{2+}–**S**]$_2$ connected to the hollow site model on Au(111) surface in the HS and the BS LS states at 300 K.

Table 2. The Current Values at 1 V of Each Orbital for [**H**–Cu^{2+}–**H**]$_2$ and [**S**–Cu^{2+}–**S**]$_2$ in the HS and the BS LS States

HS		BS	
[**H**–Cu^{2+}–**H**]$_2$			
α orbital/nA	1.45	α orbital/nA	4.82×10^{-3}
β orbital/nA	1.46	β orbital/nA	0.117
Total $(\alpha + \beta)$/nA	2.91	Total $(\alpha + \beta)$/nA	0.122
[**S**–Cu^{2+}–**S**]$_2$			
α orbital/nA	0.304	α orbital/nA	0.0356
β orbital/nA	1.51	β orbital/nA	1.20
Total $(\alpha + \beta)$/nA	1.81	Total $(\alpha + \beta)$/nA	1.22

rized in Table S1 in Supporting Information. The *I–V* curves are shown in Figure 2.

In the HS state of the [**H**–Cu^{2+}–**H**]$_2$ model, the current values for α and β orbitals at 1 V are $i_\alpha = 1.45$ nA and $i_\beta = 1.46$ nA, respectively, and the total current is $i_{\alpha+\beta} = 2.91$ nA. In Luo's approach,[43,44] the most important parameter to determine the current of the molecular wire is the coupling constant (γ). In the elastic scattering method, an electron from the source is scattered through the unoccupied molecular orbital and reaches the drain. According to frontier orbital theory, the occupied electrode orbitals mainly interact with the LUMOs of the molecule in the case of the closed-shell calculation. In that case, we have already confirmed the validity of the calculated parameter γ in our previous paper.[58] In this calculation however, the coupling constants of each end-site (1, *N*) i.e., $\gamma_{1\alpha(\beta)}$ and $\gamma_{N\alpha(\beta)}$, might be different from each other ($\gamma_{1\alpha(\beta)} \neq \gamma_{N\alpha(\beta)}$) because of the BS approach and the anti-symmetry of the molecule (In the case of a symmetric molecule, e.g., the benzenedithiol molecule, the parameters are strictly equal to each other ($\gamma_{1\alpha(\beta)} = \gamma_{N\alpha(\beta)}$).[43,44]). In the HS state of the [**H**–Cu^{2+}–**H**]$_2$ model, the γ_α value is almost equal to the γ_β value, and there is no difference in the magnitude of the current between α and β orbitals (Table 1). The overlap element, which shows the contribution of each orbital for the electrical conduction, indicates that HOMO−9, HOMO−7, and HOMO−6 for α orbital, and HOMO−8, HOMO−5, and

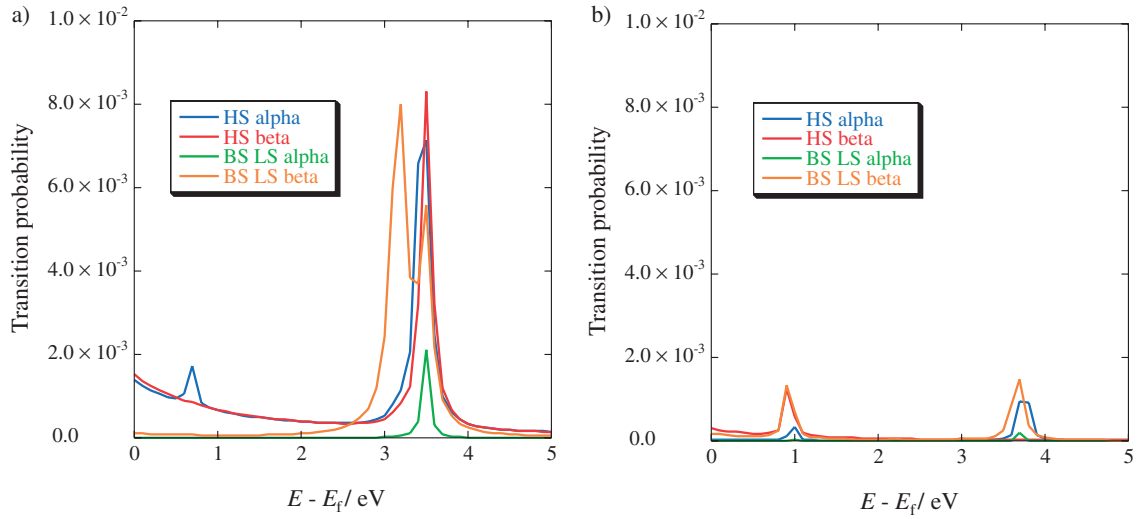

Figure 3. Transition probability of a) [**H**–Cu^{2+}–**H**]$_2$ and b) [**S**–Cu^{2+}–**S**]$_2$ connected to the hollow site model on Au(111) surface in the HS and the BS LS states.

HOMO−4 for β orbitals have a large orbital overlap as summarized in Table S1 in Supporting Information. It is found that these orbitals mainly delocalize over both the Au–S moiety and the six-membered rings, and dominantly contributes to the electron conductivity. In the BS LS state, the current values at 1 V are $i_\alpha = 4.82 \times 10^{-3}$ nA, $i_\beta = 0.117$ nA, and $i_{\alpha+\beta} = 0.122$ nA, and are different from the values of the HS state. The delocalization of molecular orbitals in the BS LS state is smaller than that of the HS state, so that the overlap element becomes very small. However, in the BS LS state of the [**H**–Cu^{2+}–**H**]$_2$ model, we found that γ_β value was much larger than γ_α value (Table 1). This behavior of the BS LS state, which is different from the HS state, is due to the fact that the β-LUMO of the isolated molecule spatially extends on the molecule more than that of the α orbital in the BS LS state.

In order to discuss the difference between the *I*–*V* characteristics in the BS LS and the closed-shell LS state, we calculated the *I*–*V* characteristics of the [**H**–Cu^{2+}–**H**]$_2$ using a restricted B3LYP (RB3LYP). We adopted the orbitals from LUMO to LUMO+2 and calculated the coupling constants. The difference of the total energies between the BS LS and the closed-shell LS is 43.2 kcal mol^{-1} and the BS LS is more stable than the closed-shell LS. The obtained current of the closed-shell LS state ($i = 1.18 \times 10^{-4}$ nA at 1 V) is much smaller than that of the BS LS state as shown in Figure S1 in Supporting Information. In the closed-shell calculation, almost all of the overlap elements are very small, indicating that the orbital delocalization of the molecule on the S atoms is smaller than that of the BS LS state. The orbital of the closed-shell LS is localized at Cu ions, whereas the HOMO of the BS LS state is delocalized on the whole molecule. In this way, the results in the BS LS and the closed-shell LS states are different, suggesting the necessity of calculations of the *I*–*V* characteristic based on static correlation such as BS method.

Next we show the results of the *I*–*V* characteristics of the [**S**–Cu^{2+}–**S**]$_2$ model. In the HS state at first, the calculated current values for α and β orbitals at 1 V are $i_\alpha = 0.304$ nA, $i_\beta = 1.51$ nA, and $i_{\alpha+\beta} = 1.81$ nA. We found that the γ_α value and the overlap element of the α orbitals are different from those of the β orbitals. The dominant overlap elements are HOMO−4 and HOMO−3 for α orbitals, and HOMO−7, HOMO−6–HOMO−4, and HOMO−3 for β orbitals. On the other hand, the current values at 1 V in the BS LS state are $i_\alpha = 0.0356$ nA, $i_\beta = 1.20$ nA, and $i_{\alpha+\beta} = 1.22$ nA. And the orbitals that mostly contributed to the electron conduction are HOMO−4 and HOMO−3 for both α and β orbitals.

These above indicates that the current of [**H**–Cu^{2+}–**H**]$_2$ tends to become larger than that of [**S**–Cu^{2+}–**S**]$_2$ in the HS states. This is because the magnitude of coupling constants between the isolated molecule and the reservoirs and the delocalization of orbitals are different in these two systems. The magnitude of the coupling constants of [**H**–Cu^{2+}–**H**]$_2$ is larger than that of [**S**–Cu^{2+}–**S**]$_2$, indicating that the interaction between the electrode orbitals and the LUMO of the molecule is stronger. It also indicates that the delocalization of the molecular orbital in [**H**–Cu^{2+}–**H**]$_2$ is larger than that of [**S**–Cu^{2+}–**S**]$_2$. It seems that this originates in the particular structure of [**S**–Cu^{2+}–**S**] type DNA. The dihedral angle between the planes defined by the aromatic rings was 22° in [**S**–Cu^{2+}–**S**] because of a crosslink by ethylenediamine in the metal–salen complex,[59] so that the overlap of the π-orbital between the adjacent base pairs becomes small and the current becomes lower.

However, in the BS LS state, the current of [**S**–Cu^{2+}–**S**]$_2$ becomes larger than that of [**H**–Cu^{2+}–**H**]$_2$. This is especially obvious at higher voltage (more than 3 V). This phenomenon is because the transition probability (Figure 3) is almost zero up to $E - E_f = 3$ (eV) in [**H**–Cu^{2+}–**H**]$_2$ in the BS LS state although it has a nonzero value even at 1 V in the case of [**S**–Cu^{2+}–**S**]$_2$. Hence the current of [**S**–Cu^{2+}–**S**]$_2$ in the BS LS state is slightly larger than that of [**H**–Cu^{2+}–**H**]$_2$.

In [**S**–Cu^{2+}–**S**]$_2$, the difference of the current values between the HS and the BS LS states is smaller than that of [**H**–Cu^{2+}–**H**]$_2$. From the distorted structure of [**S**–Cu^{2+}–**S**]$_2$, it is thought that the interaction of orbitals between adjacent base pairs is very small. Therefore, the difference in current values between the HS and the BS LS state becomes small.

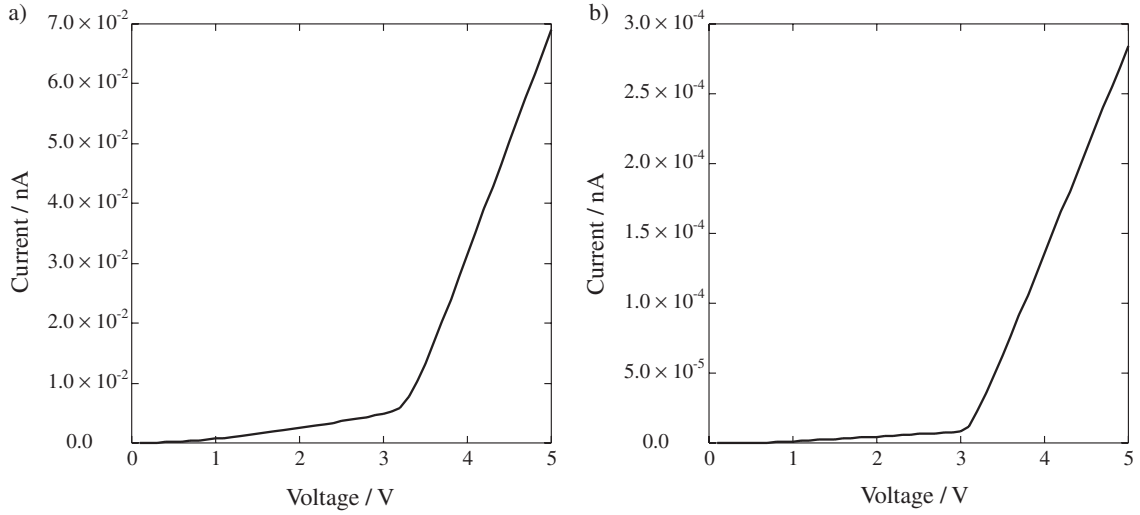

Figure 4. *I–V* curves of a) [**H**–pc–**H**]$_2$ and b) [**H**–**H**]$_2$ connected to the hollow site of Au(111) surface at 300 K.

Interestingly, in both systems, the current of the HS state is larger than the BS LS state. It originates from the interaction between the occupied electrode orbitals and the LUMO of the molecule being strong in the HS state. From eq 7, a coupling constant depends on the d value, which is the existence probability of sulfur atomic orbitals in the LUMO. In the HS state, the electron densities tend to localize around the sulfur atoms because of the spin polarization. These phenomena bring a higher current to the HS state.

Effects of Metal Ions. In order to understand the effect of Cu ions, we next examined the *I–V* characteristics without metal ions for [**H**–Cu^{2+}–**H**]$_2$. We investigated the two models without metal ions here. In one model Cu ions are replaced by the point charge (pc) (+2) ([**H**–pc–**H**]$_2$), and the other is a hydrogen bond model ([**H**–**H**]$_2$). These systems are connected to the hollow site on the Au(111) surface, as shown in Figure S2 in Supporting Information. In the [**H**–pc–**H**]$_2$ model, the geometry of all atoms is the same as that of the [**H**–Cu^{2+}–**H**]$_2$ model except for the Cu ion. In the [**H**–**H**]$_2$ model, we referred to a structure suggested in Ref. 18 and performed full optimization for this monomer structure. We used RB3LYP because there are no spin sources in the systems and they can be described by the closed-shell calculation. The distance between adjacent base pairs is assumed to be 3.7 Å. We adopted the orbitals of LUMO and LUMO+1 for calculation of the coupling constants because of the orbital degeneracy. The calculated results of the *I–V* characteristics, and γ values, the orbital energies, and the overlap elements are summarized in Figure 4 and Table S2 in Supporting Information, respectively.

The magnitudes of the current in both models are much smaller than the original models with metal ions, indicating that the coupling constant and the overlap elements are much smaller. By comparing [**H**–pc–**H**]$_2$ with [**H**–**H**]$_2$, the current of [**H**–pc–**H**]$_2$ is larger than that of [**H**–**H**]$_2$. In the case of [**H**–**H**]$_2$, the delocalization of the molecular orbital between two **H** fragments is avoided by the absence of Cu^{2+} ions, therefore the conductivity decreases. But the point charge changes an electrostatic field between two **H** fragments and the delocalization of π-orbitals, so that the conductivity is slightly increased. However, both models show much lower conductivity in comparison with models with metal ions. In this way, the introduction of Cu^{2+} ions significantly contributes to the increase of the current value.

***I–V* Characteristics of [S–Cu^{2+}–S]$_2$ with the Backbone.** Here, we examine the effect of the backbone on the *I–V* characteristics. It has been reported that the electron conductivity between the backbone and reservoirs in natural DNA is small.[11] In order to consider the effect in the artificial M–DNA, we incorporate the modeled backbone into our calculation based on the [**S**–Cu^{2+}–**S**] structure as shown in Figure S3 in Supporting Information. As a "backbone" model, we use the X-ray geometry of the metal–salen base pair complex.[59] The calculated results of the *I–V* characteristics are shown in Figure 5 and γ values, the orbital energies and the overlap elements are summarized in Table S3 in Supporting Information.

From the calculated results, we find that the magnitudes of the currents of the backbone model for the HS and the BS LS state are very small in comparison with the "without-backbone" ([**S**–Cu^{2+}–**S**]$_2$) model, indicating that the backbone cuts off the conductivity. This significant decrease of the current is simply explained by the fact that π-orbitals do not delocalize to the backbone where the electrodes are connected. This behavior agreed with the calculated result of the electron conductivity of the natural B-DNA reported by Tada et al.[11] This indicates that the "without-backbone" model for the artificial M–DNAs can transmit electricity, although a realistic model with backbone seems to scarcely conduct electrons.

***I–V* Characteristics of [H–Cu^{2+}–H] In-Plane.** We also investigated the *I–V* characteristics of the [**H**–Cu^{2+}–**H**] monomer connected to the hollow site on Au(111) surface as shown in Figure S4 in Supporting Information. This calculation represents the in-plane electron conductivity of the system. We adopted the orbitals from LUMO to LUMO+1 orbitals for the calculation of the coupling constants because of the orbital degeneracy. The calculated results of the *I–V* characteristics are shown in Figure 6 and γ values, the orbital energies and the overlap elements are summarized in Table S4 in Supporting Information.

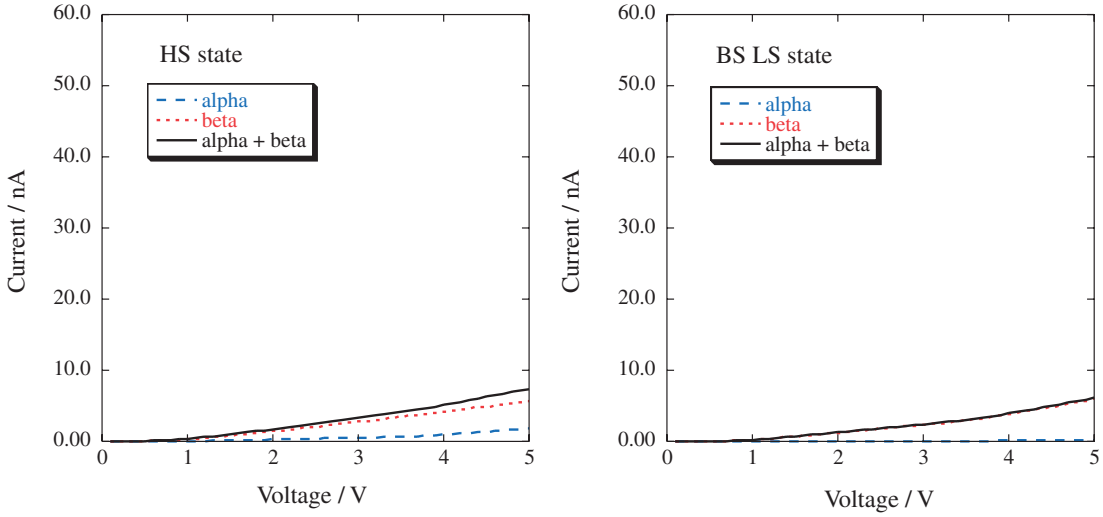

Figure 5. *I–V* curves of [**S**–Cu^{2+}–**S**]$_2$ with the backbone model connected to the hollow site of Au(111) surface in HS and BS LS states at 300 K.

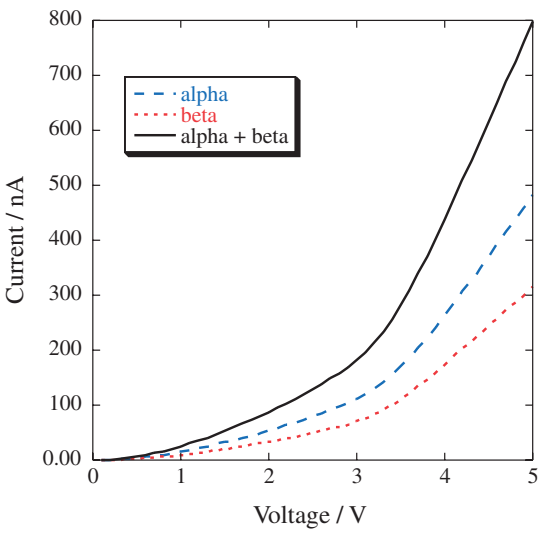

Figure 6. *I–V* curves of [**H**–Cu^{2+}–**H**] monomer model connected to the hollow site of Au(111) surface at 300 K.

From the calculated results, the magnitude of the in-plane current of the [**H**–Cu^{2+}–**H**] monomer is larger than the dimer model of [**H**–Cu^{2+}–**H**]$_2$. The reason for this high conductivity is explained as the d orbital of Cu ions assisting the π-electrons to delocalize from one hydroxypyridone to the opposite one in the same plane. In other words, the mixture of d and π orbitals causes the delocalization on the extended molecule in the plane, and then the in-plane electron conductivity becomes large. However, the Cu ion does not intermediate the delocalization between two monomers, because the distance (3.7 Å) is too long. Therefore, the conductivity between the two monomers is quite small in comparison with that of in-plane conductivity of the monomer model.

Conclusion

We investigated the *I–V* characteristics between adjacent bases in two types of artificial M–DNAs, i.e., [**H**–Cu^{2+}–**H**]$_2$ and [**S**–Cu^{2+}–**S**]$_2$, using the elastic scattering Green's function with the DFT. We focus especially on the difference between the HS and the BS LS states in the *I–V* characteristics. To our knowledge, this is the first report of comparison between them.

For this purpose, we extended the elastic scattering method reported by Luo et al. for the open-shell systems by separating the α and β spacial orbitals.

From our calculated results, we found that i) the magnitude of the current of [**H**–Cu^{2+}–**H**]$_2$ tends to become larger than that of [**S**–Cu^{2+}–**S**]$_2$, ii) the *I–V* characteristics are changed by the spin states, and iii) introduction of metal ions into DNA remarkably increases the intraplane electrical transport by increasing the delocalization of π-orbitals. These results suggest the possibility of the control of the *I–V* characteristics in artificial M–DNAs. The simple breakthrough for obtaining larger electron conductivity of artificial M–DNA seems to be replacement of a metal ion with a larger radius metal, because of the larger interaction between adjacent planes.

In our model of the stacked [**H**–Cu^{2+}–**H**]$_2$ base pairs, we use a model structure in which the backbone is replaced by S atoms connected to a Au(111) hollow site. The N–S linkages that may be very unstable in a real situation (e.g., hydrolysis) are very important for conductivity. However, our calculated results indicate that the electron transfer mainly comes from the stacked metallo-base pairs but not from the N–S linkages. If the N–S linkages dominate the electron transfer, the calculated current values should not be changed by the existence of the metal ions and by the stacking, although the calculated current values change. Therefore, the electron transfer mainly reflects the nature of the stacked metallo-base pairs.

In addition, the results also suggest that the system can be applied to spintoronics materials. Previously, our group reported the possibility of a system for molecular switching devices by an external magnetic field.[60] From both results, it seems that we can control the conductivity by changing the spin state with an external magnetic field.

Based on our approach, we compared the current of the HS state with that of the BS LS state. The results strongly indicated that the coupling constant based on the elastic scattering method drastically changed the current value.

This research has been supported by the Global COE (center of excellence) Program "Global Education and Research Center for Bio-Environment Chemistry" of Osaka University. This work has been also supported by Grants-in-Aid for Scientific Research (KAKENHI) (Nos. 19750046 and 19350070) from Japan Society for the Promotion of Science (JSPS) and Grant-in-Aid for Scientific Research on Innovative Areas ("Coordination Programming" area 2170, No. 22108515) from the Ministry of Education, Culture, Sports, Science and Technology (MEXT). This research has been also supported by a Grant-in-Aid for Core Research for Evolutional Science and Technology from the Japan Science and Technology Agency, by a Grant-in-Aid for scientific research in priority area "Molecular theory for real systems" (No. 20038008), and by a Grant-in-Aid for Young Scientists (B) (No. 20750004).

Supporting Information

Supporting data include the optimized structure of $[\mathbf{H}–Cu^{2+}–\mathbf{H}]_2$, $[\mathbf{S}–Cu^{2+}–\mathbf{S}]_2$, $[\mathbf{H}–Cu^{2+}–\mathbf{H}]$ monomer, and $[\mathbf{H}–\mathbf{H}]_2$ by UB3LYP, and structure of $[\mathbf{S}–Cu^{2+}–\mathbf{S}]_2$ with the backbone. Four tables and four figures are also given as supporting data. These materials are available free of charge on the web at http://www.csj.jp/journals/bcsj/.

References

1 V. Balzani, M. Venturi, M. Credi, *Molecular Devices and Machines: A Journey into the Nanoworld*, Wiley-VCH, Weinheim, Cambridge, **2003**.

2 C. J. Murphy, M. R. Arkin, Y. Jenkins, N. D. Ghatlia, S. H. Bossman, N. J. Turro, J. K. Barton, *Science* **1993**, *262*, 1025.

3 D. B. Hall, R. E. Holmlin, J. K. Barton, *Nature* **1996**, *382*, 731.

4 S. O. Kelley, J. K. Barton, *Science* **1999**, *283*, 375.

5 P. J. Dandliker, R. E. Holmlin, J. K. Barton, *Science* **1997**, *275*, 1465.

6 Y. Zhang, R. H. Austin, J. Kraeft, E. C. Cox, N. P. Ong, *Phys. Rev. Lett.* **2002**, *89*, 198102.

7 F. D. Lewis, T. Wu, Y. Zhang, R. L. Letsinger, S. R. Greenfield, M. R. Wasielewski, *Science* **1997**, *277*, 673.

8 M. R. Arkin, E. D. A. Stemp, R. E. Holmlin, J. K. Barton, A. Hörmann, E. J. C. Olson, P. F. Barbara, *Science* **1996**, *273*, 475.

9 D. Porath, A. Bezryadin, S. D. Vries, C. Dekker, *Nature* **2000**, *403*, 635.

10 A. Y. Kasumov, M. Kociak, S. Guéron, B. Reulet, V. T. Volkov, D. V. Klinov, H. Bouchiat, *Science* **2001**, *291*, 280.

11 T. Tada, M. Kondo, K. Yoshizawa, *ChemPhysChem* **2003**, *4*, 1256.

12 P. J. de Pablo, F. Moreno-Herrero, J. Colchero, J. G. Herrero, P. Herrero, A. M. Baró, P. Ordejón, J. M. Soler, E. Artacho, *Phys. Rev. Lett.* **2000**, *85*, 4992.

13 I. L. Zilberberg, V. I. Avdeev, G. M. Zhidomirov, *THEOCHEM* **1997**, *418*, 73.

14 N. S. Hush, J. Schamberger, G. B. Bacskay, *Coord. Chem. Rev.* **2005**, *249*, 299.

15 T. Matsui, Y. Shigeta, K. Hirao, *Chem. Phys. Lett.* **2006**, *423*, 331.

16 T. Matsui, Y. Shigeta, K. Hirao, *J. Phys. Chem. B* **2007**, *111*, 1176.

17 K. Tanaka, A. Tengeiji, T. Kato, N. Toyama, M. Shionoya, *Science* **2003**, *299*, 1212.

18 K. Tanaka, A. Tengeiji, T. Kato, N. Toyama, M. Shiro, M. Shionoya, *J. Am. Chem. Soc.* **2002**, *124*, 12494.

19 T. Kawakami, T. Taniguchi, T. Hamamoto, Y. Kitagawa, M. Okumura, K. Yamaguchi, *Int. J. Quantum Chem.* **2005**, *105*, 655.

20 H. Y. Zhang, A. Calzolari, R. Di Felice, *J. Phys. Chem. B* **2005**, *109*, 15345.

21 R. A. Jishi, J. Bragin, *J. Phys. Chem. B* **2007**, *111*, 5357.

22 Y. Nakanishi, Y. Kitagawa, Y. Shigeta, T. Saito, T. Matsui, H. Miyachi, T. Kawakami, M. Okumura, K. Yamaguchi, *Polyhedron* **2009**, *28*, 1714.

23 S. S. Mallajosyula, S. K. Pati, *Phys. Rev. Lett.* **2007**, *98*, 136601.

24 T. Matsui, H. Miyachi, T. Sato, Y. Shigeta, K. Hirao, *J. Phys. Chem. B* **2008**, *112*, 16960.

25 Y. Andersson, D. C. Langreth, B. I. Lundqvist, *Phys. Rev. Lett.* **1996**, *76*, 102.

26 G. H. Clever, K. Polborn, T. Carell, *Angew. Chem., Int. Ed.* **2005**, *44*, 7204.

27 G. H. Clever, T. Carell, *Angew. Chem., Int. Ed.* **2007**, *46*, 250.

28 Y. Nakanishi, Y. Kitagawa, Y. Shigeta, T. Saito, T. Matsui, H. Miyachi, T. Kawakami, M. Okumura, K. Yamaguchi, *Polyhedron* **2009**, *28*, 1945.

29 S. S. Mallajosyula, S. K. Pati, *Angew. Chem., Int. Ed.* **2009**, *48*, 4977.

30 G. H. Clever, S. J. Reitmeier, T. Carell, O. Schiemann, *Angew. Chem., Int. Ed.* **2010**, *49*, 4927.

31 G. H. Clever, M. Shionoya, *Coord. Chem. Rev.* **2010**, *254*, 2391.

32 K. Tanaka, G. H. Clever, Y. Takezawa, Y. Yamada, C. Kaul, M. Shionoya, T. Carell, *Nat. Nanotechnol.* **2006**, *1*, 190.

33 Y. Takezawa, W. Maeda, K. Tanaka, M. Shionoya, *Angew. Chem., Int. Ed.* **2009**, *48*, 1081.

34 J. Müller, D. Böhme, P. Lax, M. M. Cerdà, M. Roitzsch, *Chem.—Eur. J.* **2005**, *11*, 6246.

35 Y. Takezawa, K. Tanaka, M. Yori, S. Tashiro, M. Shiro, M. Shionoya, *J. Org. Chem.* **2008**, *73*, 6092.

36 F.-A. Polonius, J. Müller, *Angew. Chem.* **2007**, *119*, 5698.

37 F.-A. Polonius, J. Müller, *Angew. Chem., Int. Ed.* **2007**, *46*, 5602.

38 N. Zimmermann, E. Meggers, P. G. Schultz, *J. Am. Chem. Soc.* **2002**, *124*, 13684.

39 S. S. Mallajosyula, S. K. Pati, *J. Phys. Chem. Lett.* **2010**, *1*, 1881.

40 V. Mujica, G. Doyen, *Int. J. Quantum Chem.* **1993**, *48*, 687.

41 V. Mujica, M. Kemp, M. A. Ratner, *J. Chem. Phys.* **1994**, *101*, 6849.

42 V. Mujica, M. Kemp, M. A. Ratner, *J. Chem. Phys.* **1994**, *101*, 6856.

43 C.-K. Wang, Y. Fu, Y. Luo, *Phys. Chem. Chem. Phys.* **2001**, *3*, 5017.

44 Y. Luo, C.-K. Wang, Y. Fu, *J. Chem. Phys.* **2002**, *117*, 10283.

45 L.-L. Lin, J.-C. Leng, X.-N. Song, Z.-L. Li, Y. Luo, C.-K. Wang, *J. Phys. Chem. C* **2009**, *113*, 14474.

46 F. L. Gervasio, P. Carloni, M. Parrinello, *Phys. Rev. Lett.* **2002**, *89*, 108102.

47 E. N. Economou, *Green's Functions in Quantum Physics*, Springer, Berlin, **1990**.

48 J. R. Taylor, *Scattering Theory: The Quantum Theory of Nonrelativistic Collisions*, Wiley, New York, **1972**.

49 A. S. Davydov, *Quantum Mechanics*, NEO, Ann Arbor,

1966.

50 D. M. Newns, *Phys. Rev.* **1969**, *178*, 1123.

51 T. Dittrich, P. Hänggi, G.-L. Ingold, B. Kramer, G. Schön, W. Zwerger, *Quantum Transport and Dissipation*, Wiley-VCH, Weinheim, **1998**.

52 M. Dewar, *Bull. Soc. Chim. Fr.* **1951**, *18*, C79.

53 J. Chatt, L. Duncanson, *J. Chem. Soc.* **1953**, 2939.

54 Note that the distance of the adjacent base pair of salen-complexed DNA is very recently estimated to be 3.7 Å by Clever et al. (see Ref. 30). However, in this paper, the distance of 3.375 Å is chosen.

55 A. D. Becke, *J. Chem. Phys.* **1993**, *98*, 5648.

56 M. J. Frisch, G. W. Trucks, H. B. Schlegel, G. E. Scuseria, M. A. Rob, J. R. Cheeseman, J. A. Montgomery, Jr., T. Vreven, K. N. Kudin, J. C. Burant, J. M. Millam, S. S. Iyengar, J. Tomasi, V. Barone, B. Mennucci, M. Cossi, G. Scalmani, N. Rega, G. A. Petersson, H. Nakatsuji, M. Hada, M. Ehara, K. Toyota, R. Fukuda, J. Hasegawa, M. Ishida, T. Nakajima, Y. Honda, O. Kitao, H. Nakai, M. Klene, X. Li, J. E. Knox, H. P. Hratchian, J. B. Cross, V. Bakken, C. Adamo, J. Jaramillo, R. Gomperts, R. E. Stratmann, O. Yazyev, A. J. Austin, R. Cammi, C. Pomelli, J. W. Ochterski, P. Y. Ayala, K. Morokuma, G. A. Voth, P. Salvador, J. J. Dannenberg, V. G. Zakrzewski, S. Dapprich, A. D. Daniels, M. C. Strain, O. Farkas, D. K. Malick, A. D. Rabuck, K. Raghavachari, J. B. Foresman, J. V. Ortiz, Q. Cui, A. G. Baboul, S. Clifford, J. Cioslowski, B. B. Stefanov, G. Liu, A. Liashenko, P. Piskorz, I. Komaromi, R. L. Martin, D. J. Fox, T. Keith, M. A. Al-Laham, C. Y. Peng, A. Nanayakkara, M. Challacombe, P. M. W. Gill, B. Johnson, W. Chen, M. W. Wong, C. Gonzalez, J. A. Pople, *Gaussian 03 (Revision D.02)*, Gaussian, Inc., Wallingford, CT, **2004**.

57 H. Tatewaki, S. Huzinaga, *J. Chem. Phys.* **1980**, *72*, 399.

58 Y. Nakanishi, T. Matsui, Y. Shigeta, Y. Kitagawa, T. Saito, Y. Kataoka, T. Kawakami, M. Okumura, K. Yamaguchi, *Int. J. Quantum Chem.* **2010**, *110*, 2221.

59 G. H. Clever, Y. Söltl, H. Burks, W. Spahl, T. Carell, *Chem.—Eur. J.* **2006**, *12*, 8708.

60 Y. Shigeta, T. Kawakami, H. Nagao, K. Yamaguchi, *Chem. Phys. Lett.* **1999**, *315*, 441.